The local density approximation limit of the momentum density and the Compton profiles of Al

2004 J. Phys.: Condens. Matter 16 7363

(http://iopscience.iop.org/0953-8984/16/41/016)

INSTITUTE OF PHYSICS PUBLISHING JOURNAL OF PHYSICS: CONDENSED MATTER

J. Phys.: Condens. Matter **16** (2004) 7363–7378 PII: S0953-8984(04)81814-9

The local density approximation limit of the momentum density and the Compton profiles of Al

H Bross

Sektion Physik, University of Munich, Germany

E-mail: Helmut.Bross@cm.physik.uni-muenchen.de

Received 7 June 2004, in final form 9 September 2004
Published 1 October 2004
Online at stacks.iop.org/JPhysCM/16/7363
doi:10.1088/0953-8984/16/41/016

Abstract

In the local density approximation (LDA) the electronic structure of aluminium is calculated by use of the modified augmented plane wave method (MAPW) self-consistent scheme and the exchange–correlation functional by Vosko, Wilk and Nusair. Since the MAPW scheme produces wavefunctions especially suited for the calculation of the electronic momentum density distribution functions the improper integral defining the Compton profile (CP) $J_n(q)$ in the direction $\vec{n}$ converges well. A comparison with recent measurements of the CP along the principal directions is highly satisfying after Lam–Platzman (LP) corrections are made. In their overall shape the second derivatives of the CPs are found to be in good accord with the experimental results but give in detail no unambiguous information about the signatures of the Fermi surface breaks.

1. Introduction

The Compton profiles of Li [1, 2], Al [3], Be [4, 5], and Cu [6] have recently been measured with high resolution at least along the three principal cubic symmetry directions. The comparison of the shapes of the valence electron Compton profiles and their directional anisotropies with parameter-free theoretical predictions based on the local-density approximation established the presence of some systematic deviations: the measured profiles are always lower at low momenta, show a Fermi cut-off that is broader, and display a tail that is higher at momenta above the Fermi momentum p_F. The inclusion of exchange and correlation effects in the LDA following LAM and Platzman [7] using the occupation number density of the corresponding uniform electron gas improves the agreement slightly, but discrepancies up to 16% and 8.0% in the case of Li and of Al respectively remain. This is astonishing since the momentum density as well as the Compton profiles are ground state properties. However, we cannot expect them to have the same accuracy as the total energy and the charge density which are the central entities of the Hohenberg–Kohn theorem allowing us to determine the equilibrium lattice parameters of

fcc metals with an accuracy of less than 2%. Most of these theoretical investigations are based on, as the authors quote, highly accurate versions of the Kohn–Korringa–Rostocker (KKR) scheme which, however, show some deficiencies which might cause part of the differences between theory and experiment. Within the sphere surrounding each nucleus the standard KKR scheme produces a reliable solution of the one-particle Schrödinger equation but in the interstitial region the potential is mostly assumed to have a constant value and there exists some ambiguity with respect to the proper choice of the wavefunction compatible with the geometrical shape of the atomic polyhedron [8]. Because the wavefunctions $\langle \boldsymbol{r}|n\boldsymbol{k}\rangle$ of the standard KKR scheme are not strictly continuous at the surface of the inscribed APW sphere, the asymptotic behaviour of their Fourier transform $\langle \boldsymbol{p}|n\boldsymbol{k}\rangle$ is incorrect [9]. Thus the convergence of the improper integral determining the Compton profile

$$J_n(q) = \int_{-\infty}^{\infty} \rho(p_x, p_y, p_z = q)\,\mathrm{d}p_x\,\mathrm{d}p_y \tag{1}$$

where $\rho(\boldsymbol{p})$ is the ground state momentum density is not guaranteed. In the cited investigations this problem is avoided as the range of integration is limited to momenta up to a certain value $P_{\max}$ which is chosen to be relatively small, e.g., 5.0 au in the case of Al. In addition they suffer from the use of a non-optimal choice of the exchange and correlation functionals both in the self-consistent procedure [10] and in the evaluation of the Lam–Platzman corrections. Finally, the accuracy of the SCF scheme in [3] seems not to be very high.

The goal of the present work is to determine the extent to which the LDA correctly describes the momentum density function and the Compton profiles of Al. It is based on the MAPW scheme [11] which allows us to solve the non-interacting problem to any accuracy desired provided its characteristic parameters are properly chosen. The convergence of the improper integral in equation (1) is guaranteed because the MAPW wavefunctions as well as their first derivatives are strictly continuous everywhere [9]. In addition, the Lam–Platzman corrections are evaluated by use of the LDA charge density obtained by the self-consistent procedure. Analogous investigations by the present author [12] using the same method [13] found the directional Compton profiles of Cu and the Compton profiles of Li along different directions to be in fairly good agreement with the experimental results.

An outline of this paper is as follows: details of the MAPW scheme used to evaluate the electronic structure within the LDA are briefly sketched in the next section. Section 3 deals with the implementation of the Lam and Platzman corrections to the Compton profiles. The evaluation of the momentum densities is described in section 4. By analysing their asymptotic behaviour useful information is found which is the basis of the calculation of the Compton profiles in section 5. After an extensive comparison with experimental results some general remarks will complete this investigation.

2. Electronic structure

The band-structure problem was solved using the all-electron charge self-consistent MAPW scheme [11, 14] *ab initio*. Exchange and correlation effects were incorporated using a functional proposed by Vosko *et al* [15] which is currently considered to be the most reliable. Two characteristics favour the MAPW scheme for the present investigation.

(i) Due to additional constraints both the Bloch functions as well as their first derivatives are continuous on the surface of the APW sphere, hence their Fourier transform decays at least as $\sim 1/|\boldsymbol{p}|^4$ at large values of $|\boldsymbol{p}|$ guaranteeing the good convergence of the improper integral defined by equation (1) [9].

(ii) The density $\rho(\boldsymbol{r})$ of the electrons is a symmetric combination of a limited number of plane waves superimposed by an angle-dependent contribution within the APW sphere restricted to the angular quantum number $l \leqslant 2$.

Thus the LP corrections may be obtained in any accuracy. With respect to both the methodology as well as the accuracy achieved the present work differs from previous investigations [1–6]. As we shall see, this improved treatment is necessary to reduce the gap between theory and experiment.

For computational details we refer to the recent investigation [16] which had the result that in the case of Al the LDA is superior to the generalized-gradient approximation (GGA) as it yields the lattice with an accuracy of less than 1.2%. The present investigations have been performed at the experimental values $a = 4.031\,816$ Å $\approx 7.619\,028$ au found by extrapolating to zero temperature [17]. Apart from the energetically well separated 1s electrons all the other 11 electrons are considered as part of the MAPW scheme. The first five bands are completely occupied whereas the sixth band is occupied in most parts of the Brillouin zone. According to Bross [16], the hole Fermi surface of Al $\mathbf{h}_2$ is a truncated octahedron centred at Γ and the electron Fermi surface $\mathbf{e}_3$ consists of dumb-bells near the W points. The corresponding states belong to the seventh band which have, due to their small extension in $\boldsymbol{k}$ space, marginal influence on the momentum density and the Compton profiles. Along the directions of high symmetry $\mathbf{h}_2$ has the diameters $k_{100} = 0.923\,557$, $k_{110} = 0.928\,849$, and $k_{111} = 0.931\,131$ au which may be compared with the free-electron value $k_{\mathrm{F}} = 0.929\,611$ au. Compared to the KKR results [3] the Fermi-surface anisotropy is increased from 0.20% to 0.31%. In contrast to Schülke [2] we define the anisotropy by the standard deviation of the diameters averaged over the principal directions.

$$\delta = \sum_j g_{[j]}(k_{[j]} - k_{\mathrm{F}})^2 \tag{2}$$

with the weights $g_{100} = 0.274\,659\,25$, $g_{110} = 0.443\,802\,67$, and $g_{111} = 0.281\,538\,08$. The g have been obtained by subdividing the unit sphere into small areas and by assigning each area to one of the principal directions according to their mutual distance. They are slightly different from the values quoted by Miasek [18]. Further details on the electronic states producing characteristic features in the EMD and in the CPs are listed in table 1 which contains the possible Fermi breaks along 12 especially chosen directions in the irreducible wedge of the BZ. These orientations have been obtained by requiring that all Kubic harmonics $K_l(\boldsymbol{k}^0)$ up to $l = 34$ have non-vanishing residua in the sense as required by Bansil [19] and others [20–23]. In anticipating the considerations of section 4 the values of the EMD sum rule are listed in the last column which are more or less different from the free-electron-like value 3. For completeness the unit vectors $\boldsymbol{k}_j^0$ as well as their weights g_j, $j = 1 \cdots 12$, are given in table 1.

3. Lam–Platzman corrections of the momentum density and of the Compton profile

3.1. Basic considerations

In recent investigations there has been some controversy about the significance of the Lam–Platzman correction. Sakurai *et al* [1], Ohata *et al* [3], and Tanaka *et al* [24] mention that these corrections reduce the discrepancy between theory and experiment but that their overall effect is relatively small. However, according to Filippi and Ceperley [25], in Li they offer a satisfactory description of the electronic correlation found by Monte Carlo calculations and bring the theoretical CPs into close agreement with their experimental values.

Table 1. The unit vectors $\boldsymbol{k}^0$ of the special directions in the irreducible cubic wedge, their assigned weights, Fermi surface diameters in the direction of $\mathbf{k}^0$, in atomic units and $4\pi \int \rho(p) p^2 \, \mathrm{d}p$ along the corresponding direction.

No.	$\boldsymbol{k}_j^0$			Weight (g_j)	k_F	'Sum rule'
1	0.969 274 65	0.239 729 77	0.055 102 48	0.071 121 03	0.923 167	2.950 541
2	0.851 832 40	0.517 501 55	0.081 078 40	0.095 290 40	0.946 153	3.171 917
3	0.759 585 51	0.645 328 73	0.081 121 43	0.099 886 60	0.940 673	3.038 998
4	0.993 206 23	0.823 467 90	0.082 221 55	0.051 309 93	0.923 443	2.955 400
5	0.919 258 72	0.383 577 23	0.088 498 12	0.100 555 45		2.835 087
6	0.952 308 12	0.242 562 18	0.185 129 21	0.064 175 58	0.915 730	2.946 966
7	0.813 505 73	0.529 372 93	0.240 775 25	0.101 684 71	0.935 907	3.035 559
8	0.724 027 47	0.646 320 27	0.240 944 66	0.074 979 81	0.932 506	2.986 155
9	0.888 181 30	0.380 095 20	0.258 189 11	0.108 645 57	0.887 068	3.053 351
					0.895 306	
10	0.798 892 24	0.457 663 84	0.390 275 55	0.076 626 28	0.934 532	2.971 312
11	0.707 514 83	0.587 016 38	0.393 490 19	0.103 830 17	0.931 836	2.909 394
12	0.656 738 28	0.533 820 15	0.532 663 94	0.051 894 46	0.931 304	2.924 138

According to Lam and Platzman [7] the value of the momentum density with correlation included and its value obtained by LDA approximation differ by

$$\Delta\rho(p) = 2 \int_{V_c} \rho(\boldsymbol{r})[N_i(\rho(\boldsymbol{r});\, p) - N_f(\rho(\boldsymbol{r});\, p)] \, \mathrm{d}^3 r, \tag{3}$$

where $N_i(\rho_0,\, p)$ and $N_f(\rho_0,\, p)$ are the momentum density per electron of an interacting and a free electron gas, respectively, having the homogeneous density ρ_0. The integral extends over the unit cell and both N_i and N_f are normalized in the following way:

$$2 \int_\infty N_i(\rho_0;\, p) \, \mathrm{d}^3 p = 1 \qquad \text{and} \qquad 2 \int_\infty N_f(\rho_0;\, p) \, \mathrm{d}^3 p = 1 \tag{4}$$

to satisfy the electron number sum rule. The factor 2 accounts for the spin degeneracy.

A physically realistic model for the momentum density function $n_f = (2\pi)^3 \rho_0 N_i(\rho_0)$ has been proposed by Farid *et al* [26]. It is based on very accurate results for the correlation energy of an interacting electron gas evaluated by Ceperley and Alder [27] by use of a quantum Monte Carlo method and allows a parametrization by four quantities μ_0, μ_1, ν_0, and ν_1. For any value of the density ρ_0 we have evaluated μ_0, μ_1, and ν_1 from the listed values by use of spline interpolation; ν_0 is determined by the normalization requirement. Less sophisticated is the momentum density proposed by Cardwell and Cooper [28] which was used in the investigation [29]. It was derived by an analytic fit to the occupation number density of an interacting electron gas quoted by Lundqvist [30, 31] and has the peculiarity that $N_f(\rho_0,\, p)$ vanishes beyond $p \approx 1.51(3\pi^2\rho_0)^{1/3}$.

It is difficult to judge the quality of the way in which LP corrections have been evaluated in previous investigations. Sakurai *et al* [1] and Ohata *et al* [3] give no details at all whereas Baruah *et al* [29] use the self-consistent charge density in the muffin-tin spheres obtained from LAPW calculations but assume the density to be flat with little structure in the interstitial region.

In the present investigations the non-shape-restricted charge density $\rho(\boldsymbol{r})$ obtained from the self-consistent MAPW calculations is used without any truncation. Due to the strong variation of the charge density the $\boldsymbol{r}$-integration gives large positive and negative contributions which almost cancel each other. It is advantageous that the MAPW scheme allows us to determine the charge density at any point within the APW spheres in any desired accuracy

whereas in the remaining part of the unit cell, denoted by II, it is expressed by a sum over a small number of plane waves

$$\rho(\boldsymbol{r}) = \sum \rho(\boldsymbol{K}) \exp(\mathrm{i}\boldsymbol{K}\cdot\boldsymbol{r}). \tag{5}$$

Again the angular integration within the APW sphere can be reduced to a sum over properly chosen directions defined by the vectors $\boldsymbol{r}_j^0$ and the weights g_j as mentioned in section 2. Thus we arrive at the decomposition

$$\Delta\rho(p) = \Delta\rho_I(p) + \Delta\rho_{II}(p) \tag{6}$$

where

$$\Delta\rho_I(p) = 8\pi \sum_j g_j \int_0^{r_{\mathrm{APW}}} \rho_j(r)[N_{\mathrm{i}}(\rho_j(r);\, p) - N_{\mathrm{f}}(\rho_j(r);\, p)]r^2\,\mathrm{d}r \tag{7}$$

and

$$\Delta\rho_{II}(p) = 2\sum \rho(\boldsymbol{K}) \int_{V_{II}} [N_{\mathrm{i}}(\rho(\boldsymbol{r});\, p) - N_{\mathrm{f}}(\rho(\boldsymbol{r});\, p)] \exp(\mathrm{i}\boldsymbol{K}\cdot\boldsymbol{r})\,\mathrm{d}^3r. \tag{8}$$

$\rho_j(r)$ is the charge density along the direction $\boldsymbol{r}_j^0$. The one-dimensional integral extended over the interval $[0, r_{\mathrm{APW}}]$ must be evaluated with care since the integrand may have discontinuities at some points r_b caused by the factor $[N_{\mathrm{i}}(\rho_j(r);\, p) - N_{\mathrm{f}}(\rho_j(r);\, p)]$ which are defined by the implicit equation

$$3\pi^2\rho_j(r_b) = p^3. \tag{9}$$

As we shall see this procedure substantially smoothes the LP corrections. In accordance with the SCF calculations 24 special directions were chosen in 1/48th of the unit sphere. In domain II which for $0 \leqslant p \leqslant 1.0$ au contributes about one third to the momentum density we have applied the concept of magic points originally proposed to evaluate Brillouin zone integrals [32–34]. We found that the LP corrections of the CPs are obtained with an accuracy of 0.2×10^{-4} when 572 points are uniformly distributed in the irreducible wedge of the atomic polyhedron.

3.2. Lam–Platzman correction of the Compton profiles

Since $\Delta\rho$ only depends on the absolute value of $\boldsymbol{p}$ these corrections may be obtained from the one-dimensional integral

$$\Delta J_n(q) = 2\pi \int_q^\infty \Delta\rho(t)t\,\mathrm{d}t \tag{10}$$

where q is the projection of the momentum transfer $\boldsymbol{q}$ on the scattering direction $\boldsymbol{n}$. Due to the rapid decay of $\Delta\rho(p)$ for large values of p this integral converges quickly. Alternatively, ΔJ_n may also be expressed by the three-dimensional integral [35]

$$\Delta J_n(q) = \int_{V_c} \rho(\boldsymbol{r})[j_{\mathrm{i}}(\rho(\boldsymbol{r});\, q) - j_{\mathrm{f}}(\rho(\boldsymbol{r});\, q)]\,\mathrm{d}^3r \tag{11}$$

extended over the unit cell, where $j_{\mathrm{i}}(\rho_0;\, q)$ and $j_{\mathrm{f}}(\rho_0;\, q)$ are the CPs of the interacting and of the free electron gas of the homogeneous density ρ_0, respectively.

The momentum density function of Farid *et al* [26] yields the following expression to be inserted in equation (11):

$$j_{\mathrm{i}}(\rho_0;\, q) = \begin{cases} \pi p_{\mathrm{F}}^2\{[\mu_0 + \mu_1(1+x^2)/2](1-x^2) + \nu_0/\nu_1 \exp(-\nu_1) + \zeta/3\}, & q \leqslant p_{\mathrm{F}} \\ \pi p_{\mathrm{F}}^2[\nu_0/\nu_1 \exp(-\nu_1 x^2) + \zeta(1/x)^6/3], & q \geqslant p_{\mathrm{F}}, \end{cases} \tag{12}$$

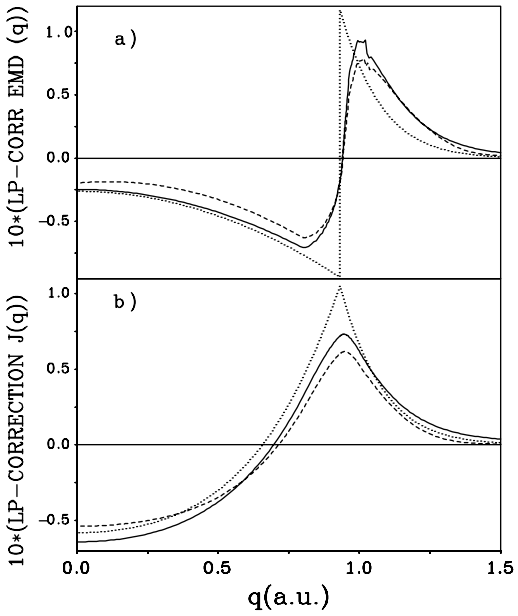

Figure 1. LP corrections of the momentum density (a) and of the Compton profile (b). Full curve, Farid *et al*; broken curve, Cardwell–Cooper; dotted curve, homogeneous electron gas with $\rho_0 = 6.592 \times 10^{-3}$ au. The EMD is in electrons/au^3, and the CP in electrons/au.

where

$$p_F = (3\pi^2\rho_0)^{1/3}, \qquad \text{and} \qquad x = \frac{q}{p_F} \tag{13}$$

and the parameters μ_0, μ_1, ν_0, ν_1,and ζ are used as defined by these authors. The analogous expression in the case of Cardwell and Cooper [28] reads

$$j_i(\rho_0; q) = \begin{cases} \pi p_F^2\{[(x^4-1)+(b+3)(b-1)/3]a/2 \\ \qquad +(x^2-1/3-2x^3/3)\delta\}, & q \leqslant p_F \\ \pi p_F^2[(b-x)^3(b+3x)/(b-1)^2]a/6, & p_F \leqslant q \leqslant bp_F \\ 0, & q \geqslant bp_F. \end{cases} \tag{14}$$

Again the authors' parameters a, b, and δ are used. Note that in contrast to the momentum density function $N_i(\rho_0; p)$ both profiles $j_i(\rho_0; q)$ are continuous at $q = p_F$ with the consequence that the integral needs no subdividing by additional break points.

3.3. Results

The LP corrections have been evaluated by using the self-consistent charge density obtained by the MAPW scheme without any further truncation. To check how various functionals N_i influence the corrections the expressions proposed by Farid *et al* (F) [26] and by Cooper and Cardwell (CC) [28] are considered. The results are displayed in figure 1 showing the corrections of the momentum density $\Delta\rho$ in the upper and the corrections of the Compton profile ΔJ in the lower panel. For comparison the LP corrections for a homogeneous electron gas corresponding to three electrons per unit cell are also displayed. It is common to both models that the correction of the momentum density has an accelerated increase in the low momentum region. As a consequence of the directional dependence of the charge density in

the crystalline case the corresponding corrections show a quite smooth variation near 0.940 au. Beyond 1.0 au the corrections derived with the F parametrization do not decay as quickly as in the case of the CC parametrization. Asymptotically they are caused by the core density. As consequence of the two-dimensional integration the corrections of the Compton profile vary more smoothly, approaching a peak at 0.9455 and 0.9476 au in the F and CC parametrization, respectively. This behaviour is to be distinctly contrasted with the case of the homogeneous gas where ΔJ has a cusp at 0.9295 au. Apart from the tail on the high momentum side the corrections caused by the two parametrizations differ from one another by a scaling factor of magnitude 1.3 or less.

4. Electron momentum density

4.1. Basic equations

In the one-particle approximation the electron momentum density is defined by the sum

$$\rho(\boldsymbol{p}) = 2\sum_{n\boldsymbol{k}} |\langle \boldsymbol{p}|n\boldsymbol{k}\rangle|^2 f_{n\boldsymbol{k}} \tag{15}$$

extended over the first Brillouin zone and over occupied states. Again the factor 2 is due to the spin degeneracy, and $f_{n\boldsymbol{k}}$ denotes the Fermi–Dirac distribution function. Many-body effects which modify $f_{n\boldsymbol{k}}$ and especially reduce the discontinuity at the Fermi energy are neglected. Completely filled bands are not influenced by this many-body aspect at all. Provided the Fourier transform of the Bloch functions is defined by

$$\langle \boldsymbol{p}|n\boldsymbol{k}\rangle = \frac{1}{(2\pi)^{3/2}} \int_{V_c} \exp(-\mathrm{i}\boldsymbol{p}\cdot\boldsymbol{r})\langle \boldsymbol{r}|n\boldsymbol{k}\rangle \,\mathrm{d}^3 r, \tag{16}$$

where V_c denotes the volume of the elementary cell; the integral of momentum density over the momentum space gives the number of electrons within the unit cell (momentum sum rule).

$$\int_\infty \rho(\boldsymbol{p})\,\mathrm{d}^3 p = 2\sum_{n\boldsymbol{k}} f_{n\boldsymbol{k}}. \tag{17}$$

As usual the Bloch functions $\langle \boldsymbol{r}|n\boldsymbol{k}\rangle$ are normalized within the elementary cell. The Fourier transform $\langle \boldsymbol{p}|n\boldsymbol{k}\rangle$ is only nonzero provided $\boldsymbol{p}$ coincides with $\boldsymbol{k}$ modulo a reciprocal lattice vector $\boldsymbol{K}$

$$\langle \boldsymbol{p}|n\boldsymbol{k}\rangle = \delta_{\boldsymbol{p},\boldsymbol{k}+\boldsymbol{K}} \times \frac{1}{(2\pi)^{3/2}} \int_{V_c} \exp(-\mathrm{i}\boldsymbol{p}\cdot\boldsymbol{r})\langle \boldsymbol{r}|n\boldsymbol{k}\rangle \,\mathrm{d}^3 r, \tag{18}$$

as a consequence of the Bloch theorem. In section 5 it will turn out to be quite advantageous that the Fourier transform of the MAPW functions approaches zero as $1/p^4$ for large values of $|\boldsymbol{p}|$ (see [9]) as a benefit of their continuity on the APW sphere. The explicit expressions of the Fourier transform given in [12] are quite adequate for numerical calculations using the MAPW results.

4.2. The momentum density along crystallographic directions of high symmetry

The momentum density along the [100], [110], and [111] directions in the especially interesting momentum interval [0.82, 1.05] au is plotted in figure 2. The broken curves displayed have been obtained from MAPW results where for each value of $\boldsymbol{p}$ a Bloch vector $\boldsymbol{k}$ within the first Brillouin zone is found by subtracting a suitably chosen reciprocal lattice vector $\boldsymbol{K}$, e.g., $\boldsymbol{p} = \boldsymbol{k} + \boldsymbol{K}$. Full curves are all-electron results with LP corrections, using the parametrization of Farid *et al* included. Contributions from the 1s, 2s and 2p electrons which are almost

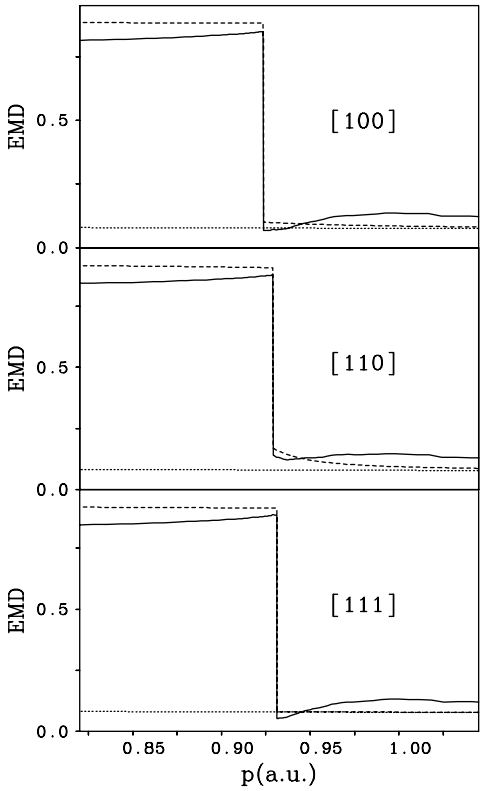

Figure 2. Electron momentum density along the [100], [110], and [111] directions. Dashed curve, all-electron LDA results; full curve, LP corrections included; lower dotted curve, core contribution. The momentum density is in electrons/au^3.

isotropic and show vary small variation in the considered interval are marked by the lower dotted curves.

Our results confirm the almost free-electronic behaviour of Al: the discontinuities in the [100], [110], and [111] directions at 0.9236, 0.9289, and 0.9311 au, respectively, correspond to the diameters of the hole-like Fermi surface $\mathbf{h}_2$. In the non-interacting picture the contribution from the valence electrons on the low momentum side slightly decreases with increasing p. Beyond the discontinuities the contributions from the rapid variations of the Bloch functions near the nuclei asymptotically merge with the contributions of the core electrons marked by the dotted curves and produce a far reaching tail. In agreement with figure 1(a) the LP corrections reduce the momentum density on the low momentum side by up to 7%. Near $p = 1.0$ au they assume maximal values and become almost comparable with the contributions of the non-interacting case. However, they have little influence on the momentum density near the discontinuities demonstrating, in the case of Al, their limited importance in simulating the many-body aspect.

4.3. The asymptotic decay of the spherically averaged momentum density: a new feature in the EMD along certain directions

To evaluate the spherically averaged momentum density we have first determined the EMD along the 12 special directions mentioned in section 2. For any directions the length p_{F}

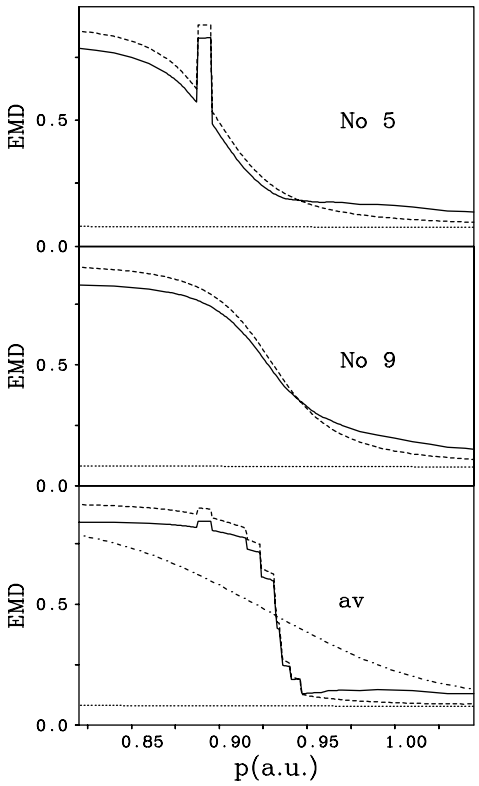

Figure 3. Electron momentum density along the special directions 5 and 9 of the 12-direction formula, and orientational averaged mean value. Dashed curve, all-electron LDA results; full curve, LP corrections included; lower dotted curve, core contribution; dashed–dotted curve, experimental result [3]. The momentum density is in electrons/au^3.

of $\boldsymbol{p}$ pointing to the Fermi surface as well as the value of the one-dimensional integral $4\pi \int_0^\infty \rho(p)p^2\,\mathrm{d}p$ are listed in table 1. Both magnitudes turn out to be quite orientation dependent. In the momentum range displayed the electronic states along directions 5 and 9 remain always below the Fermi level with the consequence that the decay of the corresponding momentum densities is quite slow as is shown in figure 3.The spike in direction 5 is caused by the seventh band which is occupied in the small momentum range [0.887 068, 0.895 306] au. In the overall view the spherical average of the momentum also plotted in figure 3 shows a smooth decay in the momentum range considered which is superimposed by small discontinuities at the Fermi breaks. To the author's knowledge such a behaviour of the averaged EMD has not yet been reported. In addition, in the lowest panel of figure 3 the spherical average of the experimental EMD is also displayed. It has been derived by use of the relation [36]

$$\rho_{\mathrm{av}}(p) = -\frac{1}{2\pi}\frac{\mathrm{d}J_{\mathrm{av}}(p)}{p\,\mathrm{d}p} \tag{19}$$

from the spherical average of the CPs along the principal directions using the corresponding weights of section 2. In the small momentum range shown it decays considerably more smoothly than the theoretical average and behaves similarly as EMDs 5 and 9. Beyond the Fermi break it approaches the theoretical EMD with LP corrections included. This is in contrast to Ohata *et al* [3] who find that the measured distribution possesses a tail higher than the theory beyond p_{F}.

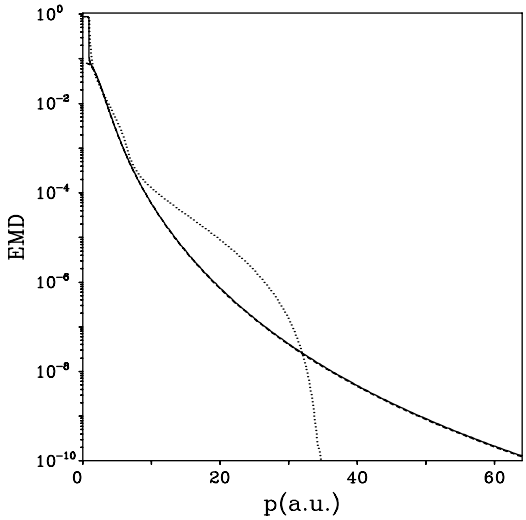

Figure 4. Full curve, spherical average of the momentum density of all electrons on a semi-logarithmic scale; dashed curve, contribution of the core electrons; dotted curve, momentum density in LDA using equation (20). Momentum densities in electrons/au^3.

Figure 4 shows the spherically averaged momentum density on a semi-logarithmic scale up to $p = 65$ au. In accordance with general considerations on the continuity of the MAPW functions we find a decay by ten orders of magnitude in the momentum range up to 65 au confirming that the MAPW Fourier transform $\langle \boldsymbol{p}|n\boldsymbol{k}\rangle$ is well suited for evaluation of the Compton profiles. On this scale the contributions to the Compton profile from all electrons and from the core electrons marked by the full curve and the broken curve, respectively, are hardly distinguishable beyond $p = 1.0$ au. It is remarkable that the momentum density in LDA obtained from the SCF-MAPW density by use of

$$\rho(p) = 2\int_{V_c} \rho(\boldsymbol{r}) N_i(\rho(\boldsymbol{r});\, p)\, \mathrm{d}^3 r, \tag{20}$$

and the all-electron spherical momentum density almost merge up to $p = 7.5$ au. At large values of p the momentum density is obviously underestimated in LDA.

Due to the strong decay of the EMD the sum rule equation (17) may be checked without any further truncations. The value 12.987 316 of the one-dimensional integral $4\pi \int_0^\infty \rho(p)\, p^2\, \mathrm{d}p$ is significantly different from the correct value 13 and is caused by the orientational dependence of the momentum density also demonstrated by the rightmost column of table 1. This view is confirmed by the fact that the spherical average of the EMDs along the principal directions gives the still smaller value 12.971 398, whereas the core electrons give the value 9.999 970.

5. Compton profile

5.1. Evaluation of two-dimensional integrals

In the so-called impulse approximation the Compton profile is defined by the two-dimensional integral over the whole plane in $\boldsymbol{p}$-space with the normal $\boldsymbol{n}$ in the scattering direction according to equation (1). A Cartesian coordinate system is introduced with the $\tilde{p}_z$-axis along the direction $\boldsymbol{n}$. To check the convergence of the improper integral defining J_n we divide the $(\tilde{p}_x, \tilde{p}_y)$-plane

by a circle of radius $P_{\max}$. The contribution to the integral from the outside of the circle where the momentum density can be assumed to be spherical is determined by

$$\Delta J_n(q) = 2\pi \int_{(q^2+P_{\max}^2)^{1/2}}^{\infty} \rho(t) t \, \mathrm{d}t \tag{21}$$

and can be evaluated in any accuracy wanted due to the asymptotic behaviour of the EMD as shown in figure 4. In accordance with the accuracy of the measured profiles [3] we require ΔJ_n to be at most 10^{-4} which implies $P_{\max} = 11.84$ au in the case of the shown ρ. Correspondingly, all momenta within the sphere of the given radius are to be considered to guarantee an accuracy of 1 part in 10^4. We have great doubts whether extending the integration over the momenta to about 5.0 au gives the accuracy of 10^{-4} as claimed by Ohata *et al* [3] since the KKR Fourier transform used by these authors certainly does not show a more rapid decay. Having this estimate in mind the evaluation of the CPs seems to be quite tedious as for each value of the momenta p the corresponding Bloch function $|n, \boldsymbol{k}\rangle$ with $\boldsymbol{k}+\boldsymbol{K} = \boldsymbol{p}$ is needed[1]. A considerable reduction of the numerical work is possible by use of a two-dimensional grid of points which are originally proposed to perform Brillouin zone integrals: the momentum space is divided into identical cubes with edges oriented parallel to the cubic [100] axis of length $\frac{1}{M}\frac{2\pi}{a}$. Their centres of gravity define a simple cubic lattice. For any value of the unit vector $\boldsymbol{n}$ there exists an orthogonal transformation which carries us to the new coordinate system $(\tilde{p}_x, \tilde{p}_y, \tilde{p}_z)$ with the consequence that the sub-manifold of the grid points having the same value $\tilde{p}_z$ form a two-dimensional lattice. Its pattern is a square, a rectangular, or a hexagonal lattice and is repeated after one, two, or three planes in the case of the [100], [110], or [111] direction, respectively [12]. Accordingly, the possible discrete values $\tilde{p}_z$ are defined by $q = \frac{1}{2M}\frac{2\pi}{a} q_{[i]} I$, where the integer $I = 0, 1 \ldots$, and $q_{[100]} = 1$, $q_{[110]} = 1/\sqrt{2}$, $q_{[111]} = 1/\sqrt{3}$. To comply with the recent experiments and the aim to reliably identify fine structures in the profiles we have chosen $M = 40$. This gives $5740\boldsymbol{p}$ points in the irreducible wedge of the Brillouin zone and almost 800 million points lying within the sphere of radius $P_{\max}$, in contrast to the $48 \times 4851 \times 177$ points considered in [3]. About one million two-dimensional $\boldsymbol{p}$ points are contained in the circle of radius $P_{\max}$ for $q \leqslant 3.0$ au. Finally the integration over the two-dimensional grid is approximated by a scheme [34] similar to that proposed by Gilat and Raubenheimer [37, 38] which allows us to take into account the exact position of the Fermi break within the corresponding parallelepipeds. To avoid spurious contributions the extension of these parallelepipeds in $\tilde{p}_z$ was chosen finite, but rather small compared to $\frac{1}{M}\frac{2\pi}{a}$.

5.2. *Comparison with experiments*

The Compton profiles of the valence electrons along the principal directions are displayed in figure 5. LP corrections have been included in the full curve. Both theoretical curves are convoluted with a Gaussian with full width at half maximum (FWHM) of 0.12 au according to Ohata *et al* [3]. For comparison the corresponding measured CPs are plotted which have slightly been renormalized, mostly by less than 0.5%, according to the theoretical results with LP corrections included. Obviously the LP corrections significantly improve the agreement with the experimental results. Apart from a narrow momentum range where the CPs manifestly vary, the LP-corrected theoretical curve and the experimental curves almost merge. This is made more clear in figure 6 where the differences between the theoretical and measured profiles along the principal directions are displayed. The uncorrected results shown in the upper panel behave quite similarly to the profiles derived with the KKR scheme [3]: at small values of q the

[1] In the case of MAPW the relation of the times needed to evaluate the Bloch function and to evaluate its Fourier transform is 30:1.

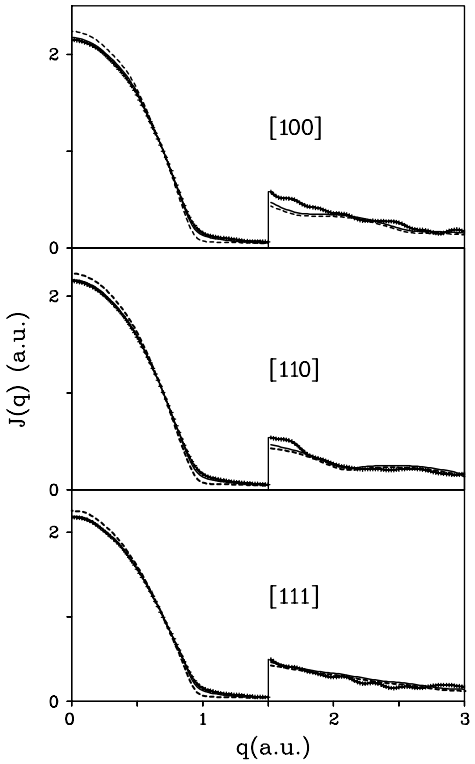

Figure 5. The valence-electron Compton profile along [100], [110], and [111]. Full curves, theoretical result with LP corrections included; dashed curves, without LP corrections; both convoluted with a Gaussian with FWHM of 0.12 au. Crosses connected by thin curves, experimental results [3]. Scale enlarged by a factor of 10 for $q \geqslant 1.5$ au.

theoretical values are overestimated up to 8% and a broad cusp occurs in the opposite direction in the momentum range [0.6, 1.2] au. As far as comparison is possible the MAPW calculations yield a small improvement of 10%. An essential step in the direction of the experimental results is due to the LP-corrections as demonstrated by panel (b). Not only in the long wave limit of the CPs but also near the cusp structures the deviations are reduced by more than a factor of 2. This allows the conclusion that in the case of Al this kind of many-body correction produces significant improvement near the Fermi surface even though the influence on the EMD is weak.

From similar investigations for $a = 7.6559$ au $= 4.051\,25$ Å corresponding to the room temperature lattice constant we have learned that a change of the temperature from 0 to 293 K will increase the CPs by $\approx$0.012 au at low momenta and by $\approx$0.006 au near p_F. At higher momenta the profiles are marginally changed. These shifts slightly worsen the behaviour shown in figure 6.

The orientation dependence of the Compton profile is quite small in the case of the free-electron metals like Al as shown in figure 7 where the profile differences along the principal directions obtained by MAPW are compared with the experimental results. By this display not only the core contributions and the many-body aspects treated by the LP procedure but also the asymptotic tail of the momentum density in the integrand of equations (1) and (21) are completely eliminated in the theoretical curves since all these contributions only depend on the absolute magnitude of the momentum $\boldsymbol{q}$. Our results are quite similar to those displayed in

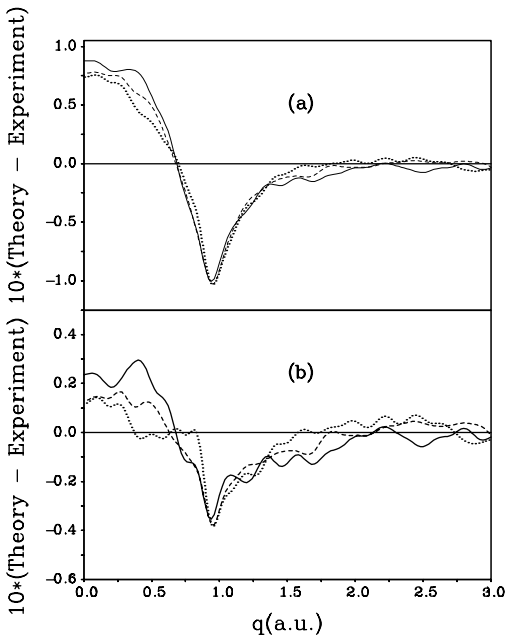

Figure 6. Differences between the calculated and the experimental valence-electron Compton profiles. (a) LDA results without LP corrections, (b) LDA results with LP corrections. Full curve, [100]; broken curve, [110]; dashed curve, [111]. See figure 5 for further details.

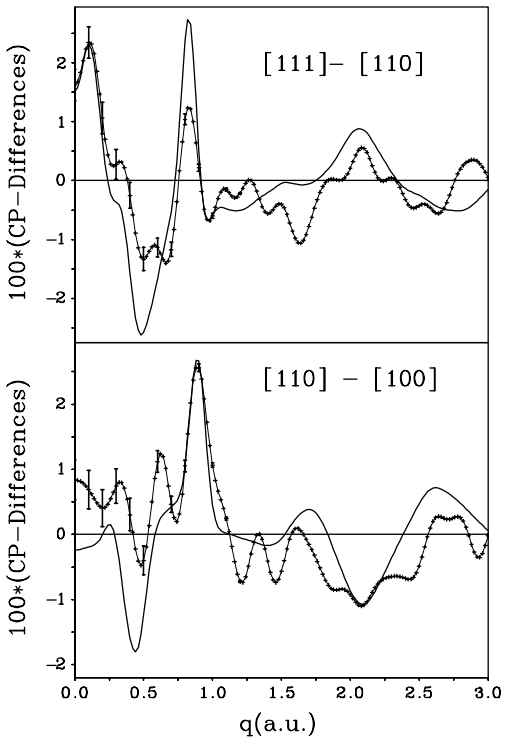

Figure 7. Directional Compton profile differences of Al. Upper panel, [110]–[100]; lower panel, [111]–[110]. Full curve, theoretical results; string of crosses, experimental data.

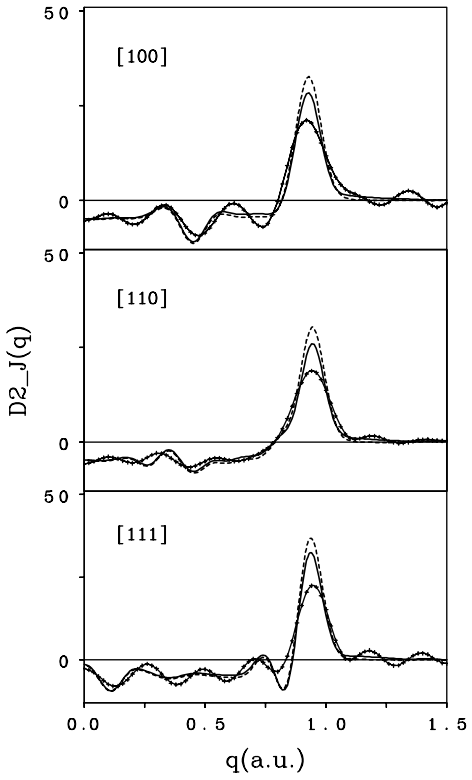

Figure 8. Second derivatives of the computed and measured profiles. Dashed curve, valence electron LDA result; full curve, LP corrections included; string of crosses, experimental data. Ordinate $\mathrm{d}^2J(q)/\mathrm{d}q^2$ in units electrons/au^{-1}. The maxima of the experimental curve are approximately located at 0.921, 0.943, and 0.947 au in the [100]-, [110]-, and [111]-direction, respectively.

figure 4 of [3] since all specific ingredients of the present investigation have only a slight effect. On the experimental side even changes caused by the renormalization of the CPs markedly influence the difference profiles. Compared to the absolute values of the profiles the agreement is satisfactory up to $q = 1.2$ au. In particular, at small values of q the difference $\Delta J_{[111]-[110]}$ coincides within the error bars with the experimental results whereas the difference $\Delta J_{[110]-[100]}$ almost completely merges near the locations of the corresponding Fermi cut-offs. Beyond this value of q the theoretical and experimental curves are rather different. In view of the smallness of the anisotropy which mostly is comparable with the accuracy of the measurement not too much significance should be attached to these discrepancies.

Both the first and second derivatives of the profiles $\mathrm{d}J(q)/\mathrm{d}q$ and $\mathrm{d}^2J(q)/\mathrm{d}q^2$ derived by spline interpolation show considerable noise which is greatly reduced by convoluting with a Gaussian of FWHM $= 0.12$ au. According to figure 8 showing the second derivatives there is good overall agreement between the theoretical and experimental curves as to both the position and the height of the peaks. On both sides of the maxima the theoretical curves smooth the wiggling feature of the experimental CPs within the error bars displayed in figure 1 of [3]. The experimental maxima are definitely broader than the FWHM $= 0.12$ au with the consequence that the heights are lowered against the theoretical results. Again the LP corrections shift the height of the maxima in the correct direction but have little influence on their position. In the

[100] and [111] directions they are located quite near to the diameters given in section 2 whereas in the [110] direction the maximum occurs near 0.944 au. Vice versa, in the [110] direction the theoretical and experimental maxima almost coincide whereas in the [111] direction the experimental maximum is shifted by $\approx$0.015 au against both the theoretical value and the KKR diameters [3], thus predicting a larger asphericity of the Fermi surface.

6. Concluding remarks

In the momentum range [0.0, 2.0] au the LP corrections of the EMD and the CPs are not marginal, but have different influences on both quantities near the Fermi break. The momentum density only undergoes a small change whereas the CPs are shifted more or less in the direction of the experimental values. Investigations along the principal directions in Al only give an incomplete picture of the orientational dependence of the momentum density. Due to the specific shape of the Fermi surface $\mathbf{h}_2$ the EMD curves within a certain range of the solid angle show no break. Up to now little attention has been paid to the fact that a crude picture of the momentum density and the Compton profiles may be already obtained in LDA by use of the momentum density of an interacting free electron gas and the non-truncated charge density of an SCF calculation. The present investigation confirms that a refined LDA calculation with LP corrections included yields the CPs, as for other ground state properties, in a wide momentum range in close agreement with measurements. It is hard to judge to what extent the remaining discrepancies are caused by many-body effects beyond the LDA or due to experimental uncertainties. In the case of Al the maxima in the second derivative of the profiles give no unambiguous information about the shape of the Fermi surface: in both the [100] and the [110] direction the Fermi surface break is properly reproduced whereas in the [111] direction a prognosis about the Fermi diameter can only be made with some reservations.

Acknowledgments

The author would like to thank Professors T Ohata and I Matsumoto for providing results of their high resolution Compton-scattering study. Dr R Bader, LRZ München, has critically read the manuscript. The generous hospitality of Professor J von Delft is gratefully acknowledged.

References

[1] Sakurai Y, Tanaka V, Bansil A, Kaprzyk S, Stewart A T, Nagashima Y, Hyodo T, Nanao S, Kawata H and Shiotani N 1995 *Phys. Rev. Lett.* **74** 2252
[2] Schülke W, Stutz G, Wohlert F and Kaprolat A 1996 *Phys. Rev.* B **54** 14381
[3] Ohata T, Itou M, Matsumoto I, Sakurai Y, Kawata H, Shiotani N, Kaprzyk S, Mijnarends P E and Bansil A 2000 *Phys. Rev.* B **62** 16528
[4] Hämäläinen K, Manninen S, Kao C-C, Caliebe W, Hastings J B, Bansil A, Kaprzyk S and Platzman P M 1996 *Phys. Rev.* B **54** 5453
[5] Itou M, Sakurai Y, Ohata T, Bansil A, Kaprzyk S, Tanaka T, Kawata H and Shiotani N 1998 *J. Phys. Chem. Solids* **59** 99
[6] Sakurai Y, Kaprzyk S, Bansil A, Tanaka Y, Stutz G, Kawata H and Shiotani N 1999 *J. Phys. Chem. Solids* **60** 905
[7] Lam L and Platzman P M 1974 *Phys. Rev.* B **9** 5122
[8] Mijnarends P E and Rabou L P L M 1986 *J. Phys. F: Met. Phys.* **16** 483
[9] Roth-Seefried H and Bross H 1977 *Z. Phys.* B **26** 125
[10] von Barth U and Hedin L 1972 *J. Phys. C: Solid State Phys.* **5** 1629
[11] Bross H, Bohn G, Meister G, Schubö W and Stöhr H 1970 *Phys. Rev.* B **2** 3098
[12] Bross H 1982 *J. Phys. F: Met. Phys.* **12** 2249

[13] Bross H 2001 unpublished investigations
[14] Bross H 2002 *Phys. Status Solidi* b **229** 1359
[15] Vosko S H, Wilk L and Nusair M 1980 *Can. J. Phys.* **58** 1200
[16] Bross H 2004 *Eur. Phy. J.* B **37** 405
[17] Figgins B F, Jones G O and Riley D P 1956 *Phil. Mag.* **1** 747
[18] Miasek M 1966 *J. Math. Phys.* **7** 139
[19] Bansil A 1975 *Solid State Commun.* **16** 885
[20] Fehlner W R and Vosko S H 1976 *Can. J. Phys.* **54** 2159
[21] Fehlner W R, Nickerson S B and Vosko S H 1976 *Solid State Commun.* **19** 83
[22] Prasad R and Bansil A 1980 *Phys. Rev.* B **21** 496
[23] Bross H 2004 unpublished
[24] Tanaka Y, Sakurai Y, Stewart A T, Shiotani N, Mijnarends P E, Kaprzyk S and Bansil A 2001 *Phys. Rev.* B **63** 045120–1
[25] Filippi C and Ceperley D M 1999 *Phys. Rev.* B **59** 7907
[26] Farid B, Heine V, Engel G E and Robertson I J 1993 *Phys. Rev.* B **48** 11602
[27] Ceperly D M and Alder B J 1980 *Phys. Rev. Lett.* **45** 566
[28] Cardwell D A and Cooper M J 1989 *J. Phys.: Condens. Matter* **1** 9357
[29] Baruah T, Zope R and Kshirsagar A 1999 *Phys. Rev.* B **60** 10770
[30] Lundqvist B I 1967 *Phys. Kondens. Mater.* **6** 193
Lundqvist B I 1967 *Phys. Kondens. Mater.* **6** 206
[31] Lundqvist B I 1968 *Phys. Kondens. Mater.* **7** 117
[32] Chadi D J and Cohen M L 1973 *Phys. Rev.* B **8** 5747
[33] Monkhorst H J and Pack J D 1976 *Phys. Rev.* **13** 5188
[34] Bross H 1978 *J. Phys. F: Met. Phys.* **8** 2631
[35] Rennert P 1981 *Phys. Status Solidi* b **105** 567
[36] Stewart A T 1957 *Can. J. Phys.* **35** 168
[37] Gilat G and Raubenheimer L H 1966 *Phys. Rev.* **144** 390
[38] Raubenheimer L H and Gilat G 1967 *Phys. Rev.* **157** 586